3-1-2008

The central component of gravitational lens Q0957+561

Deborah B. Haarsma
Calvin University

Joshua N. Winn
Harvard-Smithsonian Center for Astrophysics

Irwin Shapiro
Harvard-Smithsonian Center for Astrophysics

Joseph Lehár
Harvard-Smithsonian Center for Astrophysics

Accepted for Publication AJ

The Central Component of Gravitational Lens Q0957+561

Deborah B. Haarsma[1], Joshua N. Winn[2,3], Irwin Shapiro[3], Joseph Lehár[3,4]

ABSTRACT

In 1981, a faint radio source (G′) was detected near the center of the lensing galaxy of the famous "twin quasar" Q0957+561. It is still unknown whether this central radio source is a third quasar image or an active nucleus of the lensing galaxy, or a combination of both. In an attempt to resolve this ambiguity, we observed Q0957+561 at radio wavelengths of 13 cm, 18 cm, and 21 cm, using the Very Long Baseline Array in combination with the phased Very Large Array and the Green Bank Telescope. We measured the spectrum of G′ for the first time and found it to be significantly different from the spectra of the two bright quasar images. This finding suggests that the central component is primarily or entirely emission from the foreground lens galaxy, but the spectrum is also consistent with the hypothesis of a central quasar image suffering free-free absorption. In addition, we confirm the previously-reported VLBI position of G′ just north of the optical center of the lens galaxy. The position slightly favors the hypothesis that G′ originates in the lens, but is not conclusive. We discuss the prospects for further clarification of this issue.

Subject headings: gravitational lensing – quasars: individual(Q0957+561) – instrumentation: interferometers –

1. Introduction

When a galaxy lies close to the line of sight to a quasar, multiple images of the quasar may be produced. Almost all known lensed quasars have an even number of images—either two or four—despite a mathematical proof that nonsingular lens models always produce an odd number of images (Dyer & Roeder 1980; Burke 1981). The missing image is the "central image," corresponding to the central maximum in light-travel time. Central images are hard to detect because they are highly

[1]Calvin College, 1734 Knollcrest SE, Grand Rapids, MI 49546, dhaarsma@calvin.edu

[2]Department of Physics, Massachusetts Institute of Technology, 77 Massachusetts Avenue, Cambridge, MA 02139

[3]Harvard-Smithsonian Center for Astrophysics, 60 Garden St., Cambridge, MA 02138

[4]CombinatoRx, Inc.

demagnified by the dense core of the lensing galaxy. They are worth finding, however, because the properties of central images are unique probes of the inner 10-100 parsecs of galaxies that are too distant to resolve with ordinary observations.

Even non-detections of central images can be useful constraints on the central structure of galaxies. An upper limit on the flux density of a central image corresponds to a lower bound on the central surface density of the lens galaxy. In the context of particular galaxy models, the absence of a detectable central image can be used to set the maximum size of any constant-density core (Narasimha et al. 1986; Wallington & Narayan 1993) or the steepness of any central density cusp (Rusin & Ma 2001; Evans & Hunter 2002; Keeton 2003). Supermassive black holes also affect central images: they can prevent the formation of a central image, or produce an additional image (Mao et al. 2001; Bowman et al. 2004; Rusin et al. 2005). Microlensing by stars in the lens galaxy can demagnify a central image even further (Bernstein & Fischer 1999; Dobler et al. 2007).

Besides the faintness of the central image, there are two other reasons why it has proven difficult to identify central images. One reason is the close proximity between the expected position of the central image and the center of the lensing galaxy. The expected separation is less than $\sim$10 milliarcseconds for an isolated lensing galaxy, although it can be larger when the galaxy is part of a cluster that provides additional magnification (Inada et al. 2005). Resolving such a small separation would often require space-based imaging at optical or near-infrared wavelengths, or Very Long Baseline Interferometry (VLBI) at radio wavelengths. A second and related reason is that even when a central point source is detected, it is difficult to decide conclusively whether it is a central image of a background quasar, or an active galactic nucleus (AGN) in the lens, or a combination of these two possibilities. This decision is difficult not only because the point source is faint and challenging to characterize, but also because propagation effects may alter the properties of the central image and cause it to appear different from the other lensed images, thereby interfering with the usual tests for lensed image identification. Such propagation effects include extinction by dust at optical wavelengths, and scintillation and free-free absorption at radio wavelengths; these effects are expected to be more important for lines of sight passing very near the center of the foreground galaxy, where on average the density of dust and plasma should be greatest.

A central image was detected for the bright optical lens APM 08279+5255 (Ibata et al. 1999; Egami et al. 2000; Muñoz et al. 2001), but it seems probable that this image is the result of a highly elongated mass distribution rather than the high central density of the lensing galaxy (Lewis et al. 2002). More recently, Winn et al. (2004) presented evidence for a central image in PMN J1632–0033, thereby setting an upper limit on the mass of any central black hole and a lower limit on the central surface density of the lens galaxy. A central image has also been detected at optical wavelengths for SDSS J1004+4112 (Inada et al. 2005). In addition, there are cases in which central radio components have been detected but are most likely to be the active nucleus of the lens galaxy (Chen & Hewitt 1993; Fassnacht et al. 1999), and cases where recent work has placed stringent upper limits on the flux density of any central component (Boyce et al. 2006; Zhang et al. 2007).

This paper is concerned with the very first lensed quasar to have been discovered, Q0957+561 (Walsh et al. 1979). More than 20 years ago, a central radio component was detected in this system (Gorenstein et al. 1983), but there is still a lingering uncertainty about its interpretation. The system consists of a quasar at redshift 1.41 that is gravitationally lensed into 2 images (A and B) by an elliptical galaxy G1 and a surrounding set of galaxies mostly at redshift 0.36 (Stockton 1980; Young et al. 1981). Quasar images A and B appear as point sources in optical images and as core-jet sources in radio images. Observations with the Very Large Array (VLA) reveal a radio source, dubbed G, close to the center of the optically-identified lens galaxy G1 (Greenfield et al. 1980; Roberts et al. 1985). Radio observations with VLBI have revealed an unresolved point source near the center of G1 (Gorenstein et al. 1983). The VLBI source is known by the different name G′ because its relationship to G is unclear. The VLA and VLBI observations are sensitive to very different spatial scales of radio emission; typically, VLBI observations have an angular resolution 10-100 times finer than VLA observations and are blind to most structures that are resolved by the VLA.

Modelers of this lens have typically assumed that G′ marks the center of the lensing galaxy, and that any central quasar image is undetectably faint (see, e.g., Barkana et al. 1999; Bernstein & Fischer 1999; Chae 1999). If instead G′ is the central image, then the lens galaxy has a shallower central gravitational potential than has been assumed by those modelers. Traditionally this identification has not been a major concern, because the lens modeling literature has been preoccupied with the connection between the Hubble constant and measurements of the A–B time delay, which is not greatly affected by the innermost ∼100 pc of the galaxy mass distribution. However, as noted above, the interpretation of G′ does have an impact on our understanding of the mass distribution of the central regions of elliptical galaxies.

We undertook new radio observations of Q0957+561 in an attempt to clarify the nature of G′. Our strategy was to compare the radio spectral-energy distributions of A, B, and G′ over as large a range of radio wavelengths as feasible. For all practical purposes, gravitational lensing is wavelength-independent. Thus, the central image would have the same spectrum as images A and B, were it not for the confounding factors of intrinsic variability (in conjunction with different time delays for the different images), the magnification gradient along the jet images (in conjunction with different spectral energy distributions for the core and jets), and propagation effects specific to the line of sight of each image (such as scintillation and free-free absorption), which must be taken into account. An AGN in the lens would not have the same spectrum as the quasar images except by coincidence. Although the Q0957+561 system has been studied extensively at radio wavelengths, flux-density measurements of G′ have not been well documented. Previously, the only flux-density measurement with a reported uncertainty was by Gorenstein et al. (1983) at 13 cm. The VLA source G has been documented more completely, including measurements at wavelengths of 2 cm, 3.6 cm, and 6 cm by Harvanek et al. (1997).

In the following section, we describe our VLBI observations of this system and G′ in particular. We describe the data reduction procedures in §3, and we present the empirical results in §4. In §5

we discuss the spectrum, and in §6 we review the prospects for further progress on this issue.

2. Observations

We observed Q0957+561 with VLBI at wavelengths of 13, 18, and 21 cm. We made the 13 cm (2.27 GHz) observations over 14 hours on UT 1997 February 13, using the 10 antennas of the VLBA; the 18 cm (1.67 GHz) observations over 14 hours on UT 1997 March 19-20, using the 10 VLBA antennas and also the phased VLA and the Green Bank 140-foot telescope (since decommissioned); and the 21 cm (1.43 GHz) observations over 4 hours on UT 2005 December 30, using the 10 VLBA antennas and also the phased VLA and the Green Bank 100 m telescope. We attempted a fourth observation at 1.3 cm (22 GHz) on UT 2005 November 23, but we did not detect fringes on either the target or the chosen calibration source (J0957+5522); we do not discuss those data further.

To calibrate the relative antenna gains, we switched between Q0957+561 and a nearby, bright, and fairly compact source, J1035+5628. We used a cycling time of 5.5 minutes for the 13 cm observations, including 4 minutes spent on Q0957+561. At 18 cm we used a cycling time of 7 minutes, including 5 minutes spent on Q0957+561. Based on the results of these observations, we found that self-calibration was sufficient to calibrate the relative antenna gains, and hence for the 21 cm observations we switched to a calibration source less frequently; we visited the calibration source J0929+5013 every 15 minutes.

For all of the observations, we divided the observing bandwidth of 32 MHz per polarization into 4 sub-bands. Both senses of polarization were recorded with 2-bit sampling. The data were correlated in Socorro, New Mexico. For the 13 and 18 cm observations, we used successively three different correlation centers, chosen to match the expected locations of components A, B, and G′. For the 21 cm observations, we used two different correlation centers, chosen to match the expected locations of component A and of the midpoint between B and G′. In each case the correlation produced 16 channels of width 500 kHz from each sub-band, with an integration time of 4 seconds.

3. Data Reduction

We used standard procedures within the NRAO Astronomical Image Processing System (AIPS) for calibration, as summarized here. We discarded obviously corrupted data and data taken at elevations less than 15 degrees. We calibrated the visibility amplitudes using on-line measurements of antenna gains, system temperatures, and voltage offsets in the samplers. We removed large delay errors by fringe-fitting the data from a 1.5-minute observation of a bright calibration source at each wavelength and applying the delay corrections to all the data at that wavelength. We corrected residual rates, delays, and phases by fringe-fitting the data from J1035+5628 or J0929+5013, with a 2-minute averaging time. After calibration, we averaged the data in time and in frequency to reduce the data volume while still preserving a fine enough degree of sampling to limit the smearing

to a few per cent over the desired field of view of a few arc seconds.

We also performed self-calibration with AIPS. For each wavelength band, we created a preliminary map of the region around image A, using the CLEAN algorithm. We then self-calibrated the gain phases with reference to the CLEAN model. We repeated the process of CLEAN and self-calibration with progressively shorter averaging times until no further improvement was noted. We also attempted self-calibration of the antenna amplitudes, but only for the 18 cm data did this result in a significant improvement.

While creating our final maps, we experimented with various schemes for weighting the visibility data. In the absence of calibration and deconvolution errors, "natural" weighting based only on the expected thermal noise of each antenna should lead to a lower noise level than any other weighting scheme. This was indeed the case for the 13 cm data, which were taken with a homogeneous array of the 10 VLBA stations. However, for the 18 cm and 21 cm data, we found the best results were obtained with the AIPS parameter ROBUST = 0 (Briggs 1995), which is a compromise between natural weighting and "uniform" weighting (in which corrections are applied to give equal weight to each point in Fourier space). Apparently, the dynamic range of the 18 cm and 21 cm observations was limited to a few hundred by calibration and deconvolution errors, preventing the improvement in sensitivity from the inclusion of the larger antennas from being fully realized. In particular, for the 21 cm data, the thermal noise limit is calculated to be 20 μJy beam^{-1} for a naturally weighted map, and 32 μJy beam^{-1} for a map with ROBUST = 0. In contrast, our best map (obtained with ROBUST = 0) has an rms noise level of 45 μJy beam^{-1}. The best indication that the problem is indeed dynamic range comes from the Stokes Q map, in which the peak flux density is much smaller than in the I map and the noise level is much closer to the theoretical limit. Similar conclusions based on similar data have been reached by Boyce et al. (2006) and Zhang et al. (2007). For the final maps, we simultaneously deconvolved the fields around both A and B, to prevent sidelobes from image B from lowering the dynamic range in the vicinity of A, and vice versa.

To characterize the jet structures of quasar images A and B, we also created a set of maps at 18 cm using uniform weighting of the visibility data and a circular restoring beam of radius 4 mas after deconvolution. These maps are shown in Figure 2 (and were previously reported by Haarsma et al. 2000). They have rms noise of 55 (67) μJy beam^{-1} in the vicinity of A (B). The ROBUST = 0 maps had a lower noise level in presumably blank regions of the sky, but for jet characterization we prefer the uniformly weighted maps because uniform weighting provides a better suppression of the sidelobes. The circular restoring beam also allows for a visual comparison to previous work.

4. Results

We successfully detected G′ at 13 cm, 18 cm, and 21 cm. We measured the flux density of G′ by fitting a point-source model to the final maps (using the AIPS task JMFIT). The measured component flux densities and map rms noise are given in Table 1. Fitting G′ with a two-dimensional Gaussian function did not change the results significantly, indicating that G′ was unresolved by our observations. Thus there is no evidence for a jet or any additional structure in G′ larger than the size of the synthesized beam. The principal axes of the synthesized elliptical beam (in milliarcseconds) and the position angle of the major axis (east from north) at 13 cm, 18 cm, and 21 cm are 5.8×4.3 ($-13°$), 7.4×5.5 ($-11°$), and 14×5.2 ($1\overset{\circ}{.}7$), respectively. In addition, there are no sources in the $1.2'' \times 1.2''$ region around G′ brighter than 4σ above the noise.

We also measured the total flux densities of A and B at each epoch, using the sum of the flux density within an aperture that encompassed the bright point source and the jet (using the AIPS task TVSTAT). These results are also given in Table 1. There is some subjectivity involved in defining the aperture that encompasses the entire jet; based on the results from apertures of different sizes and shapes, we find the uncertainty in the total flux densities of A and B to be about 5%.

At 13 cm, we measured the flux density of G′ to be 0.83 ± 0.07 mJy. Gorenstein et al. (1983) measured the 13 cm flux density of G′ to be 0.60 ± 0.10 mJy based on data obtained in 1981, an observation sixteen years earlier than ours. The difference in the two results is 0.23 ± 0.12 mJy, suggesting that G′ is variable, but this difference may also be due to the two sets of VLBI data being from different arrays and being calibrated by different means.

The coordinates we measured for G′ at each wavelength agree with each other and with the coordinates reported by Gorenstein et al. (1983) within 1σ; hence, we confirm the previously reported position. A compilation of reported coordinates for G′, G, and G1 is given in Table 2 and plotted in Figure 2. Notably, the most precise positions of G′, G, and G1 are in disagreement at the 2-3σ level, and in particular G′ is located north of the optically detected lens galaxy G1.

The jets of A and B shown in Fig. 2 at 18 cm appear similar to those presented by Garrett et al. (1994) (hereafter G94), but with some intriguing differences described below. Due to the difficulties described in §3 in achieving the thermal noise limit, these maps do not have a significantly better signal-to-noise ratio than the G94 maps. Moreover, the component most significant for modeling (component 5 of G94, the brightest part of the jet), did not change significantly in location, brightness, or position angle in the 8 years between the G94 observations and our observations. Thus, the new maps are unlikely to provide significant improvement in the magnification matrix of the lens, and hence we have not attempted to provide a comprehensive quantitative description of the jet maps.

Campbell et al. (1995) monitored the jets from 1987 to 1993 with an angular resolution of about 1 mas and did not detect any motion of the components along the jets. Our jet maps do,

however, suggest some small but interesting changes in the jets between 1989 and 1997 (marked on Figure 2). These differences are not much more significant than spurious noise features, but they could suggest superluminal motion of the jet components. In A and somewhat in B, the region 5-20 mas from the core is somewhat brighter in 1997 than in 1989, perhaps as component 2 of G94 moved further from the core. In A, the region about 65 mas from the core (component A6 in G94) is brighter, and in B, a new component has appeared on the end of the jet. These slight changes are not definitive enough to be useful, but we do caution lens modelers to account for possible superluminal motion when calculating uncertainties in the magnification matrix, as noted by Barkana et al. (1999).

5. The Spectrum of G′

Our goal was to clarify the origin of G′ by comparing the broad-band radio spectrum of G′ with that of A and B, over as wide a range of wavelengths as possible. As noted in the introduction, gravitational lensing itself is achromatic, leading to the expectation that lensed images have the same dependence of radio flux density on wavelength, with the caveats that intrinsic variability, magnification gradients across the source, and propagation effects are confounding factors.

We examine the flux-density ratios G′/B and A/B, rather than the flux densities themselves, because the ratios are not subject to the extra uncertainty introduced by the overall flux-density calibration when comparing results from different epochs. The solid symbols plotted in Fig. 3 represent the VLBI measurements from this work as well as the 13 cm VLBI measurements by Gorenstein et al. (1983). (The open symbols are discussed below.) The top panel shows the ratio A/B, while the bottom panel shows G′/B; in both cases the axes are logarithmic, with identical horizontal axes and vertical axes that both span a factor of 10. Clearly, G′/B decreases significantly with wavelength. If the radio spectrum of each component is described by a power law, $S_\nu \propto \nu^\alpha$, then a least-squares fit of a straight line on the logarithmic plot shows that the exponents for G′ and B differ by $\Delta\alpha = -1.04 \pm 0.23$. At face value this suggests G′ has a different spectrum from B and is therefore not the central quasar image. A proper interpretation, however, requires consideration of several additional factors.

One factor is the intrinsic variability, coupled with the time delays. The quasar is known to be variable in luminosity at 6 cm and 3.6 cm by as much as 30% (Lehár et al. 1992; Haarsma et al. 1997, 1999). This variation is slow compared to the A-B time delay, varying by at most 15% over 1.1 years. Because of the time delays, each image displays the quasar in a different luminosity state, and thus the instantaneous flux-density ratio may vary. For images A and B at 3.6 cm, this variation of A/B could be as large as ±15%. This effect could account for some of the 30% difference between our 1997 measurement of the 13 cm A/B flux density ratio and the 1981 measurement of the same quantity by Gorenstein et al. (1983). The measurements of A/B at other wavelengths, observed on a variety of dates, are consistent within ∼20% across the spectrum.

The time delay between the central image and the B image is expected to be much shorter than the delay between the A and B images, since the time delay depends on the image positions roughly as $\Delta\tau_{BA} \propto r_B^2 - r_A^2$ (Kochanek 2002), where r denotes the angular distance from the image to the lens center. If G′ is the central image, its distance from the lens is less than $0\farcs01$, while A and B are at $r_A \sim 5''$ and $r_B \sim 1''$, respectively. Since the time delay between A and B is ~ 1.1 years (Haarsma et al. 1997; Kundić et al. 1997; Oscoz et al. 1997; Schild & Thomson 1997), the delay between B and G′ would be less than one month. At radio wavelengths, the most rapid observed variation of the quasar has been ∼2% per month, and the typical variation is even slower (Haarsma et al. 1999). Since the measurement uncertainty for the flux ratio is ∼4%, variability should not significantly affect our interpretation of the spectrum of G′/B.

Another factor is the gradient in magnification along the extent of the VLBI jets (*e.g.* Garrett et al. 1994; Barkana et al. 1999), coupled with the different radio spectra of the core and jets. These factors will cause the sum of the core and jet flux densities to vary with wavelength in a manner specific to each quasar image (Conner et al. 1992). Thus, the flux ratio of the two images will appear to be wavelength dependent if the core and jet are combined. For Figure 3, we calculated the flux ratios using the sum of the core and jet flux density for each image, because the jet of the central image would be less than 1 mas long and unresolved by our measurements.

How much would the magnification gradient affect the G′/B spectrum? The magnification of the central image and its jet depends on the unknown central mass distribution of the lens. Many other key parameters are known, however, or can be derived from observations, such as the spectral indices and magnifications of the core and jet in the A and B images. Assuming that the flux density of G′ is due entirely to the central image and its jet, we tested a range of values for the ratio of the G′ jet magnification divided by the G′ core magnification. This ratio is expected to be greater than 0.8 in simple models; we tested a wide range of values from 0.8 to 1.6. Holding the 18 cm flux densities fixed, we found the difference between the G′/B ratio at 21 cm and the G′/B ratio at 2 cm to be altered by less than 10%. Thus, it is unlikely that the magnification gradient is introducing variations in the G′/B spectrum at a level above 10%.

A final factor that may affect the G′/B spectrum is the possibility of differential propagation effects. G′ may suffer more from propagation effects due to its proximity to the center of the lens. Whether G′ is radiation from the lens or the quasar, its measured flux density may be affected by free-free absorption and/or scintillation due to ionized material near the lens's center. Therefore we must consider the possibility that G′ is at least in part a central image whose spectrum has been altered by propagation effects. This issue can be addressed by checking for the characteristic wavelength dependence of these effects (for example, the optical depth due to free-free absorption is expected to vary roughly as λ^2), or preferably, by observing at short enough wavelengths that propagation effects are expected to be negligible, as done by Winn et al. (2004) for PMN J1632–0033. Since our 1.3 cm VLBI observations that were intended for this purpose did not succeed, below we compare our results with previous VLA observations at shorter wavelengths.

As mentioned above, VLA observations revealed a central radio source G that is located near the center of the optically detected galaxy G1. Component G is unresolved by the VLA, save for faint north-south extensions (Roberts et al. 1985; Harvanek et al. 1997) reminiscent of a core and two-sided jet of a low-luminosity AGN. Comparisons of the flux density of G and G′ must be made with caution because of the very different spatial scales involved; the VLA observations had a beam size of 300-1000 mas as compared to the 3-10 mas beam size of the VLBI observations. To the VLA, G′ is unresolved and its flux density must contribute fully to the total measured flux density of G. However, the flux density of G′ as measured by the VLBI arrays does not include any of the structure that has been resolved by the VLA, and is also missing an unknown fraction of the flux density of G that is unresolved by the VLA but that is resolved out on even the shortest baselines of the VLBI array.

Harvanek et al. (1997) decomposed G into three subcomponents: an unresolved point source, a northern extension, and a southern extension. The two extensions were referred to as "remnants." Harvanek et al. (1997) provided estimates of the flux density of each of the three subcomponents at 6 cm and 3.6 cm. At 2 cm, they did not detect the remnants and provided only the flux density of the unresolved subcomponent. In the absence of shorter-wavelength VLBI data, we assumed for present purposes that the unresolved portion of G is the appropriate comparison to G′. The open symbols in Fig. 3 show the measurements by Harvanek et al. (1997). In the lower panel, we set the error bars equal to the quoted flux density of the brighter of the two remnants, since there is likely to be a strong correlation in the measured flux densities of each of the three subcomponents.

Unfortunately, the short-wavelength VLA measurements of G′/B do not resolve the issue. The data are consistent with a model of free-free absorption (dotted line in Fig. 3) in which G′/B varies as $\exp(-\tau_\nu)$ with $\tau_\nu \propto \nu^{-2.1}$ (Mezger & Henderson 1967). A least-squares fit has a χ^2 of 7.7 and 6 degrees of freedom. The data are also consistent with a model in which G′ is the lens AGN with a different power-law spectrum than B and no free-free absorption (solid line in Fig. 3). The best least-squares fit of a straight line to G′/B has a χ^2 of 6.4 and 6 degrees of freedom. Thus, according to this analysis, we cannot rely on the current spectrum to distinguish between the two models, especially in light of the possible systematic errors in the G/G′ correspondence.

6. Future Prospects for Understanding G′

Although we have measured the spectrum of G′ for the first time, the source of G′ remains ambiguous. In this section, we review the relevant observations relating to G′, and we consider the prospects for clarifying the nature of G′ with future observations. Clearly, one way forward would be to fill in the short-wavelength part of the spectrum with VLBI observations with a high signal-to-noise ratio at several wavelengths. In addition, several other observable properties of G′ could be useful, namely, its overall brightness, position, radio structure, and variability. We treat each of these in turn.

Overall brightness.—It has long been argued that G′ is unlikely to be a central quasar image based on its brightness. Its measured flux density is reasonable for a low-luminosity AGN (Roberts et al. 1985) but brighter than simple lens models would predict for the central image. For example, assuming that the central mass distribution of G1 is approximately isothermal, the central image C should be demagnified by approximately r_C/r_E relative to the bright quasar images, where r_C is the distance from the central image to the lens center and r_E is the Einstein radius. Since r_C is likely to be less than 10 mas and r_E is roughly 3000 mas, one would expect demagnification by a factor of 300 rather than the factor of 30-50 we measure for G′. (Note that if G′ is a combination of the central image and the lens galaxy nucleus, they must be separated by a fraction of a milliarcsecond to appear unresolved in our data, and at such a separation the central image would be even more strongly demagnified.) However, apart from the uncertainty in the position of G1 relative to G′, we are reluctant to attach much weight to this argument because it involves some circular logic: after all, it is the mass distribution of the lens galaxy that we are trying to study. The order-of-magnitude argument given here also does not take into account the mass-sheet degeneracy (Falco et al. 1985) and other inherent limitations of lens modeling.

Position.—Most realistic lens models would predict that the central image should be located closer to image B than to image A. In such cases, it should fall south of G1, roughly along the line joining G1 and B. In contrast, an AGN of the lens galaxy is expected to lie very close to the center of G1, although there is no guarantee that a central black hole marks the precise center of mass. Still, there is the potential to distinguish between these possibilities with a very accurate measurement of the G′–G1 angular separation and position angle. In this work, we confirm the Gorenstein et al. (1983) VLBI position of G′. The most precise optical position of G1 comes from *HST* observations (Bernstein et al. 1997) (see Table 2 and Figure 1). The separation between these measurements of G′ and G1 is 10.6 mas, about three times larger than the measurement uncertainty (3.6 mas, dominated by uncertainty in the optical centroid of G1). A 3σ measurement is not precise enough to conclusively confirm or deny that G′ and G1 are coincident. The position angle, however, is more suggestive. G′ lies to the *north* of G1, contrary to the expectation that the central image would appear south of the lens. Thus, the position information slightly favors the hypothesis that G′ is the AGN of the lens galaxy.

It is not clear whether future *HST* data or other data will allow for a significant improvement, but measuring the position of G1 more accurately is a potentially promising avenue for future progress. The detection of an optical point source displaced from the center of G1 would be an excellent candidate for the optical counterpart to G′ and good evidence for a central image, just as it is for the lens system SDSS J1004+4112 (Inada et al. 2005). The existing *HST* data show a power-law surface brightness distribution with no evidence for an additional central point source down to $\sim 0\farcs1$. The non-detection of an optical counterpart to G′, even at a level smaller than 1% of A, does not rule out the central-image hypothesis because the optical central image can be made much fainter than the radio central image due to microlensing by stars or extinction by dust.

Radio structure.—If G′ is a third quasar image, then it is demagnified by a factor of 30-50

relative to images A and B. Since A and B are observed to have jets that extend out to ∼50 mas in VLBI maps, the corresponding jet in G′ is expected to have an extent of ∼1 mas. This is a factor of a few smaller than the synthesized beam of our VLBI observations, which means that the pointlike appearance of G′ in our maps is not constraining. Rogers (1988) reported a core-jet structure for G′, but this finding is not confirmed by our study, nor by any published study we are aware of. Furthermore, although the detection of a slight extension in G′ would certainly be interesting, one would want to see the detailed correspondence between that jet and the jets of A and B before declaring G′ to be the central image. Otherwise, it could represent a jet from the AGN in the lens, or the combination of a central image and an AGN. This test would require considerably greater angular resolution and sensitivity.

The VLA component G, in contrast, is certainly resolved on ∼500 mas scales (Harvanek et al. 1997), which is much larger than the lensing expectation. Furthermore, investigators have observed extended, low-surface-brightness radio lobes about 15″ to the north and south of G1, oriented along nearly the same direction as the extension of G (Avruch et al. 1997; Harvanek et al. 1997). These seem like clear indications that G must include at least some contribution from an AGN in the lens galaxy G1. Harvanek et al. (1997) noted some problems with this interpretation, mainly that the morphology of G1 would not be that of a typical radio galaxy of either of the two Faranoff-Riley categories. They raised the possibility that at least some of the extended structure near G actually originates from image B and represents the counter-jet to the long and prominent arcsecond-scale jet of image A, but this interpretation is also problematic. In any case this issue is somewhat separate from the issue of the identity of the VLBI component G′, except insofar as the knowledge that G1 is definitely an active galaxy would raise the likelihood that G′ is its radio nucleus.

Variability.—The background quasar is known to be variable; thus the central image C should also vary and have the correct time delay relative to the A and B images (although the B-C time delay would be much shorter than the A-B delay, as discussed above). Source G was not seen to vary significantly in our VLA monitoring (Lehár et al. 1992; Haarsma et al. 1997, 1999) and G′ has had no consistent observations to detect variation. Even if G′ were shown to vary, that would not conclusively prove it is the central image, since the radio core of the lens could also be variable. The observation of correlated variability would be required to show that G′ is the central image. Since A and B are at least occasionally variable at the 30% level, one would want to detect variations of G′ at that level with a high signal-to-noise ratio.

Such an undertaking is probably too demanding on current resources to be feasible, but it will be feasible with the next generation of radio observatories. As an example we consider the *Expanded Very Large Array* (EVLA), an effort to improve almost all of the relevant observing parameters of the VLA by a factor of 5-20. With the VLA, G can be detected at 2 cm with a signal-to-noise ratio of 8 in a 6 hr observation (Harvanek et al. 1997). With a factor of ∼10 improvement in the 2 cm band, the EVLA could obtain a signal-to-noise ratio of 20 in about 4 hr (if the dynamic range is not as limited as we experienced with a heterogeneous VLBI array). This measurement could be repeated every few weeks for a few years to search for correlated variability, although the

configuration changes of the VLA would complicate the actual observing plan. Of course the whole strategy depends on the assumption that at 2 cm the flux density of G is dominated by that of G′, an assumption that can be checked in future VLBI observations. Further developments in high-sensitivity VLBI, along with the advent of the Atacama Large Millimeter Array and eventually the Square Kilometer Array can also be brought to bear on this stubborn problem.

D.H. acknowledges the support of Calvin College and a Cottrell College Science Award from Research Corporation.

REFERENCES

Avruch, I. M., Cohen, A. S., Lehár, J., Conner, S. R., Haarsma, D. B., & Burke, B. F. 1997, ApJ, 488, L121

Barkana, R., Lehár, J., Falco, E. E., Grogin, N. A., Keeton, C. R., & Shapiro, I. I. 1999, ApJ, 520, 479

Bernstein, G. & Fischer, P. 1999, AJ, 118, 14

Bernstein, G., Fischer, P., Tyson, J. A., & Rhee, G. 1997, ApJ, 483, L79

Bowman, J. D., Hewitt, J. N., & Kiger, J. R. 2004, ApJ, 617, 81

Boyce, E. R., Winn, J. N., Hewitt, J. N., & Myers, S. T. 2006, ApJ, 648, 73

Briggs, D. S. 1995, PhD thesis, New Mexico Institute of Mining and Technology

Burke, W. L. 1981, ApJ, 244, L1

Campbell, R. M., Lehár, J., Corey, B. E., Shapiro, I. I., & Falco, E. E. 1995, AJ, 110, 2566

Chae, K.-H. 1999, ApJ, 524, 582

Chen, G. H. & Hewitt, J. N. 1993, AJ, 106, 1719

Conner, S. R., Lehár, J., & Burke, B. F. 1992, ApJ, 387, L61

Dobler, G., Keeton, C. R., & Wambsganss, J. 2007, MNRAS, 377, 977

Dyer, C. C. & Roeder, R. C. 1980, ApJ, 241, 133

Egami, E., Neugebauer, G., Soifer, B. T., Matthews, K., Ressler, M., Becklin, E. E., Murphy Jr., T. W., & Dale, D. A. 2000, ApJ, 535, 561

Evans, N. W. & Hunter, C. 2002, ApJ, 575, 68

Falco, E. E., Gorenstein, M. V., & Shapiro, I. I. 1985, ApJ, 289, L1

Fassnacht, C. et al. 1999, AJ, 117, 658

Garrett, M. A., Calder, R. J., Porcas, R. W., King, L. J., Walsh, D., & Wilkinson, P. N. 1994, MNRAS, 270, 457

Gorenstein, M. V., Shapiro, I. I., Cohen, N. L., Corey, B. E., Falco, E. E., Marcaide, J. M., Rogers, A. E. E., Whitney, A. R., Porcas, R. W., Preston, R. A., & Ruis, A. 1983, Science, 219, 54

Greenfield, P. E., Roberts, D. H., & Burke, B. F. 1980, Science, 208, 495

Haarsma, D. B., Hewitt, J. N., Lehár, J., & Burke, B. F. 1997, ApJ, 479, 102

—. 1999, ApJ, 510, 64

Haarsma, D. B., Lehár, J., & Barkana, R. 2000, in Gravitational Lensing: Recent Progress and Future Goals, held at Boston University, July 1999, ed. T. G. Brainerd & C. S. Kochanek (San Francisco: ASP)

Harvanek, M., Stocke, J. T., Morse, J. A., & Rhee, G. 1997, AJ, 114, 2240

Ibata, R. A., Lewis, G. F., Irwin, M. J., Lehár, J., & Totten, E. 1999, AJ, 118, 1922

Inada, N. et al. 2005, PASJ, 57, L7

Keeton, C. R. 2003, ApJ, 582, 17

Kochanek, C. S. 2002, ApJ, 578, 25

Kundić, T. et al. 1997, ApJ, 482, 75

Lehár, J., Hewitt, J. N., Roberts, D. H., & Burke, B. F. 1992, ApJ, 384, 453

Lewis, G. F. et al. 2002, MNRAS, 334, L7

Mao, S., Witt, H. J., & Koopmans, L. V. E. 2001, MNRAS, 323, 301

Mezger, P. G. & Henderson, A. P. 1967, ApJ, 147, 471

Muñoz, J. A., Kochanek, C. S., & Keeton, C. R. 2001, ApJ, 558, 657

Narasimha, D., Subramanian, K., & Chitre, S. M. 1986, Nature, 321, 45

Oscoz, A., Mediavilla, E., Goicoechea, L. J., Serra-Ricart, M., & Buitrago, J. 1997, ApJ, 479, L89

Roberts, D. H., Greenfield, P. E., Hewitt, J. N., Burke, B. F., & Dupree, A. K. 1985, ApJ, 293, 356

Rogers, A. E. E. 1988, in Gravitational Lenses: Proceedings, Cambridge, Massachusetts, 1988, ed. J. M. Moran, J. N. Hewitt, & K. Y. Lo, Lecture Notes in Physics No. 330 (Springer-Verlag), 77

Rusin, D., Keeton, C. R., & Winn, J. N. 2005, ApJ, 627, L93

Rusin, D. & Ma, C. 2001, ApJ, 549, L33

Schild, R. & Thomson, D. J. 1997, AJ, 113, 130

Stockton, A. 1980, ApJ, 242, L141

Wallington, S. & Narayan, R. 1993, ApJ, 403, 517

Walsh, D., Carswell, R. F., & Weymann, R. J. 1979, Nature, 279, 381

Winn, J. N., Rusin, D., & Kochanek, C. S. 2004, Nature, 427, 613

Young, P., Gunn, J. E., Kristian, J., Oke, J. B., & Westphal, J. A. 1981, ApJ, 244, 736

Zhang, M., Jackson, N., Porcas, R. W., & Browne, I. W. A. 2007, MNRAS, 377, 1623

Table 1. Total flux densities of components

Component	13 cm		18 cm		21 cm	
	Total (mJy)	RMS (mJy)	Total (mJy)	RMS (mJy)	Total (mJy)	RMS (mJy)
A	43.34	0.06	41.72	0.03	34.12	0.05
B	25.59	0.06	23.41	0.04	22.86	0.05
G′	0.83	0.07	0.53	0.03	0.46	0.05

Table 2. J2000 positions of the central component relative to image B

Right Ascension (arcseconds)		Declination (arcseconds)		Source	Instrument	Reference
0.19	±0.03	1.00	±0.03	G1	optical ground	Stockton 1980 (S80)
0.1820	±0.0035	1.0178	±0.0035	G1	optical HST	Bernstein et al. 1997 (B97)
0.155	±0.001	1.050	±0.001	G	radio VLA	Roberts et al. 1985 (R85)
0.16	±0.01	1.03	±0.01	G	radio VLA	Harvanek et al. 1997 (H97)
0.185	±0.001	1.028	±0.001	G′	radio VLBI	Gorenstein et al. 1983 (G83)
0.1844	±0.0015	1.0278	±0.0020	G′	radio VLBI	this work

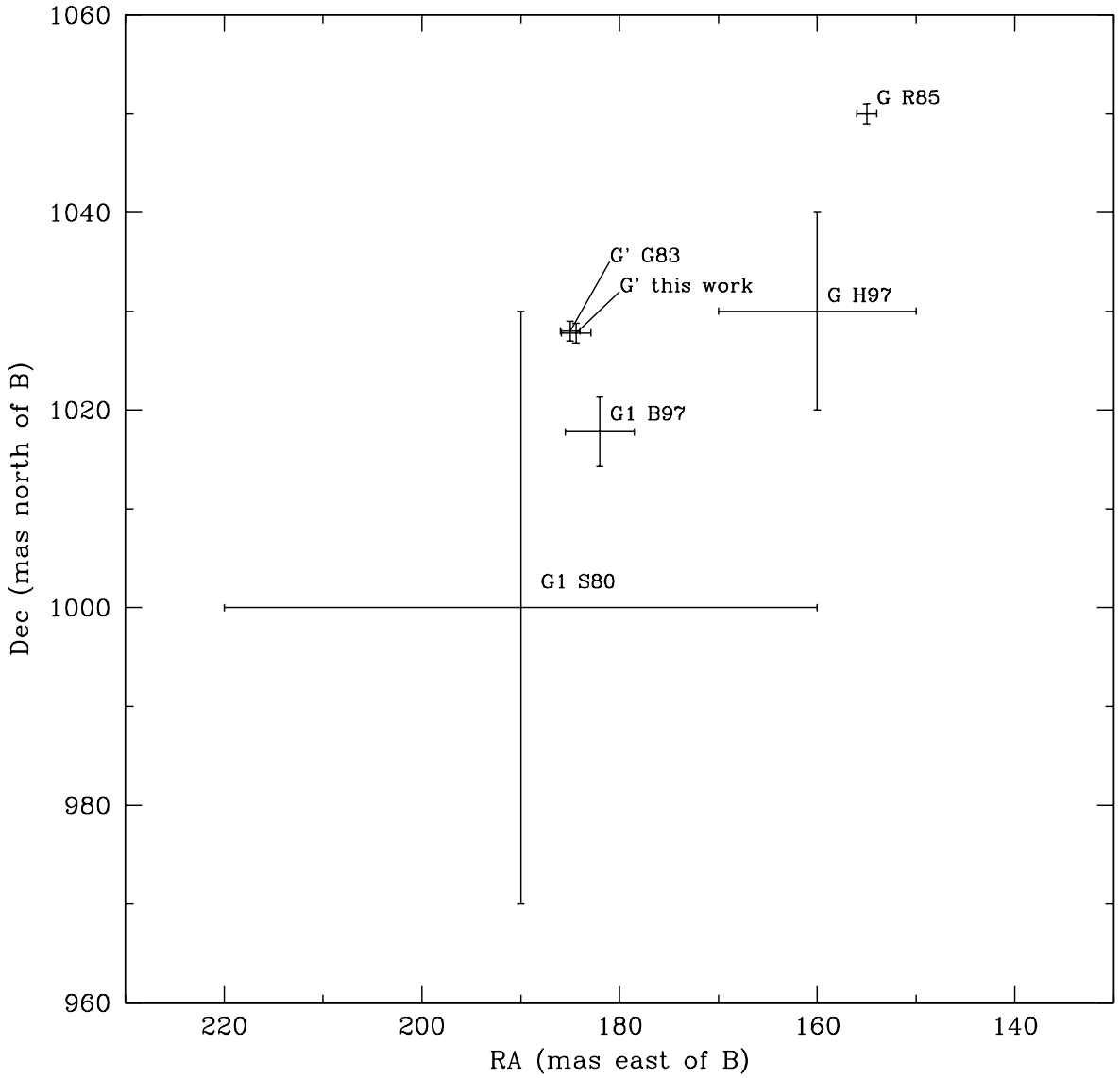

Fig. 1.— Positions of optical lens galaxy G1, radio VLA source G, and radio VLBI source G′ (see Table 2 for references). Note that Roberts et al. (1985) indicate that the uncertainty in their position is underestimated; the Harvanek et al. (1997) uncertainties are more typical for positions found with the VLA.

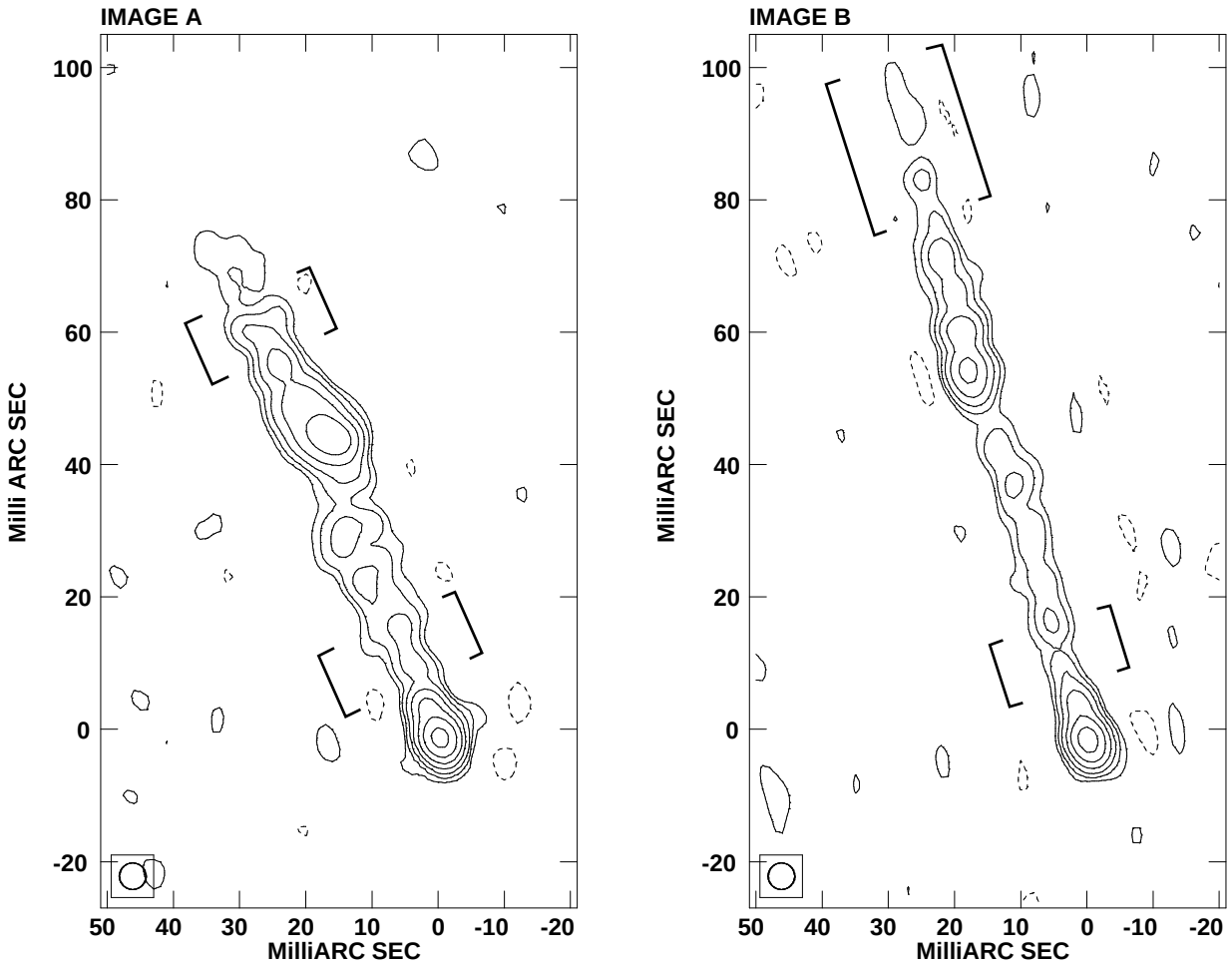

Fig. 2.— Maps of images A and B at 18 cm as observed on 1997 Mar 19-20. The coordinates of map A (B) are centered at J2000 10:01:20.69 +55:53:55.6 (10:01:20.84 +55:53:49.6). The contours are at flux densities of -0.15,0.15, 0.3, 0.6, 1.2, 2.4, 2.8, 9.6 mJy beam^{-1}. The 4 mas circular restoring beam is shown in the lower left. Brackets indicate regions that appear brighter in 1997 than in the 1989 observations by Garrett et al. (1994).

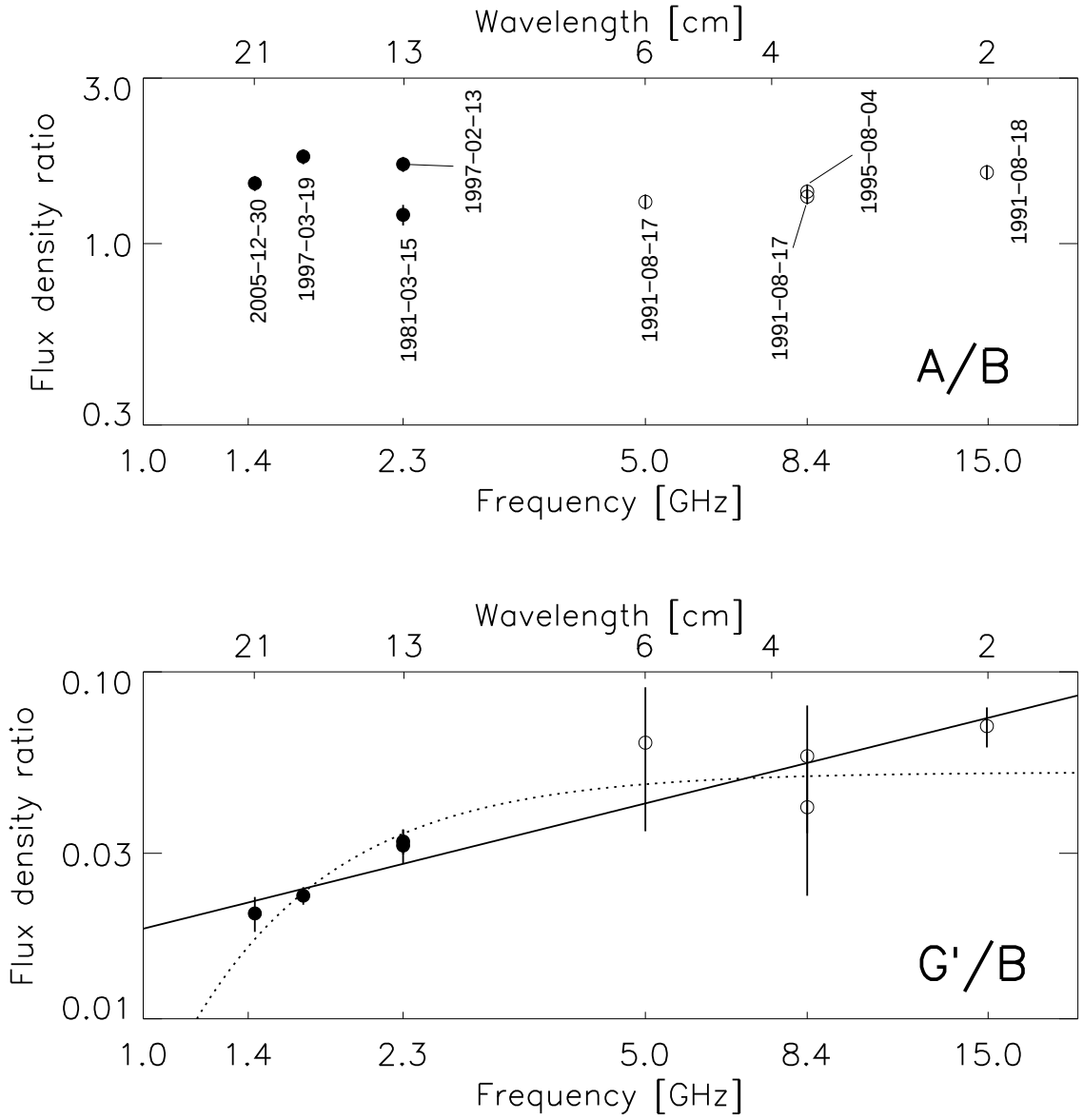

Fig. 3.— The flux-density ratios A/B (top panel) and G′/B (bottom panel) as a function of observing wavelength. The observing dates are displayed in the top panel. The data points at wavelengths shorter than 10 cm (open symbols) are for the VLA component G measured by Harvanek et al. (1997), while those points at longer wavelengths (filled symbols) are for the VLBI component G′ measured in this work and at 13 cm by Gorenstein et al. (1983). In the top panel, A/B is seen to vary significantly, which can be at least partially attributed to intrinsic variability and the differential time delay (see § 5). In the bottom panel, the dotted curve is the best fitting 2-parameter model in which G′ is a central image suffering free-free absorption ($\tau_\nu \propto \nu^{-2.1}$) in the lens galaxy. The solid line is the best-fitting 2-parameter model in which G′ is an AGN in the lens galaxy with a different power-law spectrum than that of the quasar images.